Photothermal triggering of self-healing processes applied to the reparation of bio-based polymer networks

2016 Mater. Res. Express 3 045003

(http://iopscience.iop.org/2053-1591/3/4/045003)

Materials Research Express

RECEIVED
15 December 2015

REVISED
12 February 2016

ACCEPTED FOR PUBLICATION
10 March 2016

PUBLISHED
1 April 2016

PAPER

Photothermal triggering of self-healing processes applied to the reparation of bio-based polymer networks

F I Altuna[1], J Antonacci[2], G F Arenas[2], V Pettarin[1], C E Hoppe[1] and R J J Williams[1]

[1] Institute of Materials Science and Technology (INTEMA), University of Mar del Plata and National Research Council (CONICET), Av. J. B. Justo 4302, B7608FDQ, Mar del Plata, Argentina

[2] Laser Laboratory, Physics Department, Engineering Faculty, University of Mar del Plata, J.B. Justo 4302, B7608FDQ, Mar del Plata, Argentina

E-mail: faltuna@fi.mdp.edu.ar

Keywords: polymeric nanocomposite, photothermal effect, self-healing

Supplementary material for this article is available online

Abstract

Green laser irradiation successfully activated self-healing processes in epoxy-acid networks modified with low amounts of gold nanoparticles (NPs). A bio-based polymer matrix, obtained by crosslinking epoxidized soybean oil (ESO) with an aqueous citric acid (CA) solution, was self-healed through molecular rearrangements produced by transesterification reactions of β-hydroxyester groups generated in the polymerization reaction. The temperature increase required for the triggering of these thermally activated reactions was attained by green light irradiation of the damaged area. Compression force needed to assure a good contact between crack faces was achieved by volume dilatation generated by the same temperature rise. Gold NPs dispersed in the polymer efficiently generated heat in the presence of electromagnetic radiation under plasmon resonance, acting as nanometric heating sources and allowing remote activation of the self-healing in the crosslinked polymer.

Introduction

The development of self-healing polymers has experienced an enormous advance in the last decade, as research on this topic gained both scientific and industrial interest. Conceived with the aim to extend the service life of structural and functional polymers, these materials are capable of mending cracks, either upon the application of external stimuli or by themselves, thus restoring the original (or at least similar) mechanical properties [1–3].

Several methods to manufacture self-healing thermosetting polymers are well described in literature, including thermoplastic/thermoset mixtures [4–6] as well as composites containing microcapsules [7], or vascular systems [8, 9] filled with polymer precursors, initiators or catalysts, which are released when a crack propagates throughout the material. An alternative approach is the introduction of reversible or dynamic covalent bonds in the polymeric networks, leading to intrinsically self-healing polymers [3]. Thermosets with reversible Diels–Alder adducts, that can be depolymerized by increasing the temperature, were one of the first chemistries studied, accounting for a significant proportion of the existing literature [10, 11]. More recently, a wide variety of chemical groups such as β-hydroxyesters [12–14], disulfides [15, 16], acylhydrazones [17], urea [18], or vinylogous urethanes [19], among others, were successfully employed, giving birth to a new class of polymers, termed 'vitrimers'. These materials can suffer a topology change by activation of dynamic reactions in a temperature range located above the glass transition, which depends on the specific material and on the presence or not of catalysts, and without changing the average number of covalent bonds of the polymer network. These self-healable crosslinked polymers also offer the possibility of being reprocessed and even recycled, making them a very promising alternative for many diverse applications [12, 19].

Light activation of self-healing processes could provide remote spatial and temporal control on the stress relaxation and mending of the material, adding an extra value to the innovative chemical design and applications of bio-based crosslinked networks [20]. The effect of light irradiation will depend on the chemistry and

composition of the material. Photo-crosslinking reactions, photoinduced metathesis or material heating are some of the possible effects that can induce the initiation of a self-healing process when a material is irradiated [20]. The use of the photothermal effect would have the advantage of potentially producing high temperatures increases in localized areas, which could extend remote activation to thermosetting polymers (with a high glass transition temperature, T_g, or degree of crosslinking) and to chemistries based on rearrangements of dynamic covalent bonds, requiring relatively high temperatures to be activated.

The photothermal effect observed in nanostructures of certain metallic materials is recognized as a very efficient way to exchange luminous energy into heat. The effect is a consequence of the surface plasmon resonance, and takes place when the metallic nanostructures are excited by photons of a specific frequency, matching that of their plasmon resonance [21, 22]. The characteristic plasmon resonance frequency for nanoparticles (NPs) of a given metal can be tuned by selecting the appropriate shape and size [23–25]. Besides spherical NPs, several anisotropic nanostructures displaying more than one plasmon resonance frequency can be synthesized to induce the photothermal effect using light sources within a very wide range of wavelengths [24, 25].

The photothermal effect can be applied for the remote triggering of smart polymeric materials, such as shape memory or self-healing polymers, by including low amounts of metal NPs to the polymer matrix. Provided the poor thermal conductivity of polymers, high temperatures increases could be obtained even with moderate power sources [26]. Thermal profiles and peak temperatures are expected to be controlled by the nature, size and shape of NPs as well as by the composition, physicochemical characteristics of the polymer matrix and power of the light source employed. The photothermal effect has already been applied to trigger the response of shape-memory polymers [20, 27, 28], and to the self-healing of soft hydrogels and semi-crystalline polymers [29–32]. However, to our knowledge, there are no current available studies on the application of this effect to the remote activation of self-healing of bio-based polymer networks with relatively high crosslinking degrees.

Here, we describe the synthesis and properties of a nanocomposite obtained by embedding gold NPs in a bio-based polymer network with dynamic covalent bonds. This material is the result of the merging of the aforementioned research fields, and is intended to be a proof of concept for the design of remotely activated self-healing chemically crosslinked polymers. The bio-based polymeric amorphous network is obtained by the crosslinking of epoxidized soybean oil (ESO) with citric acid (CA), and the self-healing ability of the matrix achieved through the exchange of β-hydroxyester bonds [13]. Polyvinylpyrrolidone (PVP), a nontoxic and biocompatible polymer, is used to functionalize gold NPs that, in the way of aqueous colloidal dispersions, can be easily incorporated to the polymeric matrix precursors.

The analysis of some relevant thermal and physical properties is discussed and the assessment of the remotely activated self-healing using laser irradiation is shown in detail. Both qualitative and quantitative methods were employed to test the performance of these materials, with the aim of demonstrating the feasibility of inducing the healing of the polymeric matrix by a novel approach, and highlighting its advantages over traditional ones.

Experimental

Materials

Epoxidized soybean oil (ESO; iodine value = 2.4; EEW = 241 g/eq; average molecular weight = 940 Da; average functionality = 3.9 epoxides per triglyceride) was kindly supplied by Unipox S.A. (Buenos Aires, Argentina). Citric acid (CA) monohydrate ($C_6O_7H_8.H_2O$; ⩾98.0%), hydrogen tetrachloroaurate (III) ($HAuCl_4.3H_2O$; ⩾49.0% Au basis), sodium citrate tribasic dihydrate ($C_6O_3H_5Na_3.2H_2O$; 99%) and polyvinylpyrrolidone (PVP; number average molecular weight = 10 000 Da) were purchased from Sigma-Aldrich. All chemicals were used as received without any further purification. A representative chemical structure of ESO and the chemical structures of CA, sodium citrate and PVP are shown in figure 1.

Synthesis of ESO-CA networks

The synthesis of ESO-CA networks with a stoichiometric ratio R = (carboxylic acid equivalents)/(epoxy equivalents) of 0.5 was described and discussed elsewhere [13]. Typically, 2.178 g of an aqueous solution of CA (4 parts by weight of CA monohydrate with 1 part of distilled water) was prepared at 90 °C and added to 12.0 g of ESO at 90 °C, with continuous stirring. After 10 min, the solution was cast into a glass mold covered with anti-adherent paper, and it was placed in a convection oven (Yamato DKN400). The polymerization was performed for 6 h at 90 °C and 12 h at 120 °C. The post-curing step at 160 °C for 4 h was carried out outside the mold.

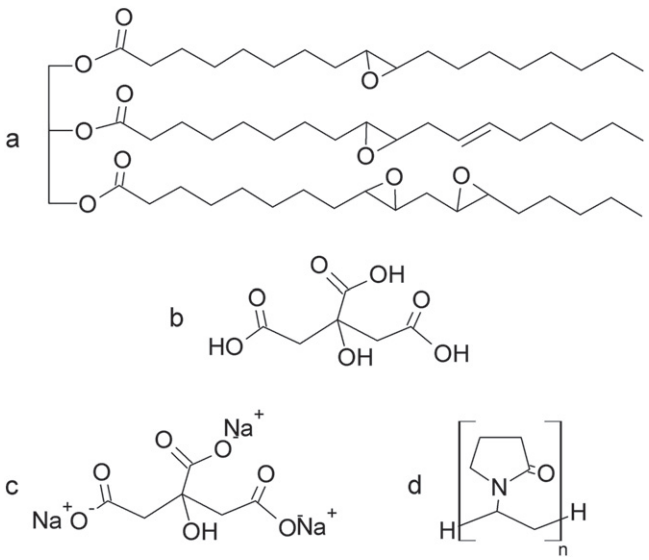

Figure 1. Representative chemical structure of ESO (a) and chemical structures of CA (b), sodium citrate tribasic (c) and PVP (d).

Synthesis of Au NPs

PVP capped Au NPs (Au@PVP) were synthesized by post-functionalization of gold NPs obtained by the Turkevich method [33]. Briefly, 3.40 ml of an aqueous $HAuCl_4$ solution (0.036 52 mol l^{-1}) were diluted in 250 ml of water and heated until boiling. Subsequently, 12.5 ml of 1% (w/v) sodium citrate solution were added, and heating and stirring were maintained for 30 min. The dispersion was left to cool to room temperature before adding 10 ml of 26.5% (w/v) PVP aqueous solution. The mixture was stirred for 24 h, and Au@PVP NPs were separated by centrifugation (4 times; 1 h; 600 rpm) to obtain an aqueous dispersion of NPs with an average diameter of 13.1 nm and a standard deviation of 2.7 nm. A more detailed analysis of the NPs size distribution is available in the supplementary data file.

Synthesis of ESO-CA-Au@PVP nanocomposites

The incorporation of Au@PVP NPs to the ESO-CA matrix was performed in a two-steps procedure. First, an aqueous dispersion of Au@PVP NPs was added to 12.0 g of ESO at 90 °C. This mixture was stirred for 15 min at 90 °C to evaporate the water. The second step was the addition of an aqueous CA solution as it was done for the neat ESO-CA networks. For this system, the pre-polymerization step was performed for 15 min to assure a better elimination of water. The curing program was the same as that used for the neat polymers (6 h at 90 °C, 12 h at 120 °C and a post-curing of 4 h at 160 °C outside the mold). The obtained nanocomposites were labeled as ESO-CA-Au@PVP (0.08) and ESO-CA-Au@PVP (0.02), where the numbers between brackets indicate the Au content as wt%.

Methods

UV-visible absorption spectra were obtained with an Agilent 8453 UV–vis spectrophotometer. A 1 cm wide quartz cuvette was used for the measurement of Au@PVP NPs water dispersions, whereas specimens between 1.5 and 2.0 mm thick were used for the neat ESO-CA polymer and for the nanocomposites.

The Au@PVP NPs distribution in the ESO-CA matrix was examined by transmission electron microscopy (TEM). Thin nanocomposite samples were cut by crio-ultramicrotomy and images were taken with a JEOL JEM-1011 microscope, operated at 100 kV.

Shear stress relaxation rate was determined for ESO-CA-Au@PVP (0.02) nanocomposite and for the neat polymer. Isothermal tests were performed at 160 °C on specimens of rectangular cross-section (2 mm × 5 mm) in an Anton Paar Physica MCR 301 rheometer, using a torsion fixture with a distance between clamps equal to 17.4 mm. When the sample reached the test temperature, a 5% torsional deformation was applied and the relaxation modulus, $G(t)$, was recorded. Stress relaxation was assessed from the variation of G/G_0 with time, where G_0 is the initial modulus. The same specimen dimensions and configuration were used to perform dynamic mechanical analysis (DMA) tests, at a heating rate of 2 °C min from −50 to 170 °C with a fixed frequency of 1 Hz.

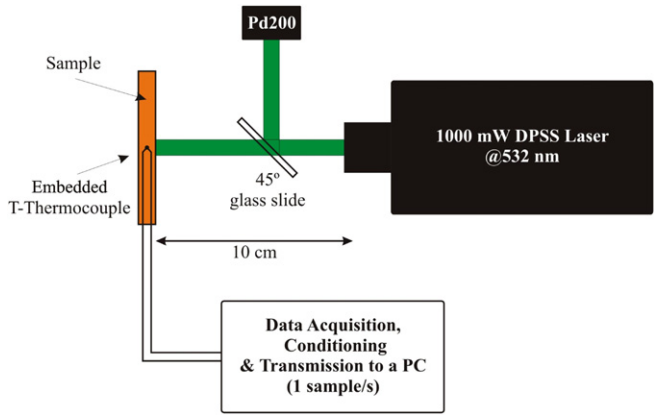

Figure 2. Experimental set-up used for the assessment of the photothermal effect, and the crack healing.

The photothermal effect was studied by illuminating specimens of the ESO-CA-Au@PVP nanocomposites from a distance of 10 cm with a 1000 mW DPSS green laser (SDL-532–1000T Shanghai Dream Lasers Technology Co. Ltd; $\lambda = 532$ nm) operated using a power control. A maximum output power of 700 mW at the sample location, on an irradiated area of 0.4 cm^2 (corresponding to a diameter of 7 mm), was indirectly measured using an Ophir PD200 silicon sensor. Temperature was recorded every 1 s for different laser intensities using an embedded T-type thermocouple, constructed with thin wires (0.18 and 0.27 mm), and placed at a distance of about 0.8 to 0.9 mm of each face of the specimen, as close as possible to the center of the sample. The same procedure was carried out for the neat ESO-CA networks to evaluate the temperature increase due to the matrix absorption. Figure 2 shows a scheme of the experimental set-up.

The efficiency of the self-healing remote activation was assessed both qualitatively and quantitatively. Damage reparation was examined through direct observation, and with a Leica DMLB transmission optical microscope (TOM). Mechanical tests were carried out in order to estimate the degree of reparation achieved. Prismatic strips, cut from virgin and repaired samples, were used to prepare uniaxial tension specimens of $2 \times 5 \times 40$ mm^3. Polypropylene tabs were bonded at the specimen ends to avoid specimen collapse between grips. The space between the extended parts of the tabs was filled in with high modulus elastomeric ribs. Tensile tests were carried out at 18 °C in an Instron 4467 universal Testing Machine at a cross-head speed of 5 mm min^{-1} until complete breaking of the specimens.

Results and discussion

ESO-CA-Au@PVP cured samples were pink-colored and homogeneous to the naked eye, with no visible evidences of macro-aggregation or extended clustering. Figure 3 shows the distribution of NPs within the ESO-CA-Au@PVP nanocomposites as obtained by TEM. Chain-like/elongated arrangements, along with a small population of randomly dispersed NPs, could be observed in every analyzed region of sample ultrathin cuts. Reasons for the spontaneous self-assembly of NPs in one-dimensional structures are not completely clear, especially in the case of non-magnetic, spherical nanostructures [34–36]. In our case, the experimental evidence is also insufficient to explain the origin of this preferential anisotropic arrangement. However, some previous results could contribute to understand this quite unexpected behavior.

First of all, a change in the polarity and dielectric constant of the NPs dispersion medium associated with the transfer from water to the ESO-CA reactive system is expected to provoke a modification of the energetic balance and interactions among NPs, favoring chain-like assembling. Some studies conducted in simple solvents, like ethanol, showed that dipole–dipole interaction could be the main driving force for the formation of this kind of structures. Under conditions in which intrinsic, or induced, dipole–dipole interactions are strong enough to overcome the thermal energy and the electrostatic repulsion between the colloidal particles, chaining occurred [35]. Presence of PVP as stabilizing agent could also favor linear arrangement, as has been observed in the one-dimensional organization of gold clusters on plain surfaces. In this case, a mechanism in which nanoclusters act as junctions between PVP chains was postulated [37]. Finally, as a consequence of the decrease in the contribution of the entropy of mixing occasioned by the increase in the average molar mass of the polymer, probability of phase separation enhances with the advance in polymerization reaction [38]. This effect has been identified as responsible for the formation of cluster-like, self-assembled arrangements of NPs in the polymerization of reactive blends modified with NPs [39, 40].

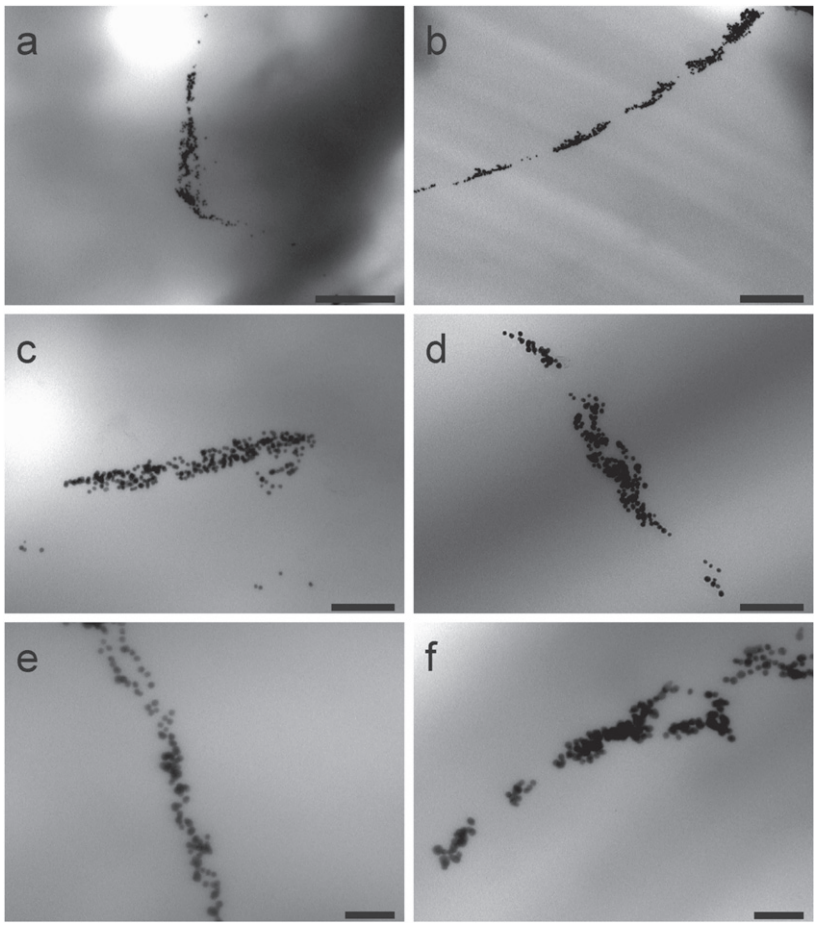

Figure 3. TEM micrographs at different magnifications, obtained from ultrathin sections of ESO-CA-Au@PVP (0.02) (pictures (a), (c) and (e)) and ESO-CA-Au@PVP (0.08) (pictures (b), (d) and (f)) samples. Scale bars lengths represent 500 nm (pictures (a) and (b)), 200 nm ((c) and (d)) and 100 nm ((e) and (f)).

All the factors mentioned above would favor a phase-separated morphology, in which NPs-rich domains will be dispersed in the rich-polymer continuous phase. In the present case, selected conditions seem to favor anisotropic interactions in a way conducting to the formation of elongated/chain-like arrangements with a typical length of several hundreds of nanometers.

Presence of linear arrangements of NPs dispersed in the network was also evidenced by UV–vis spectrophotometric measurements. UV–vis spectra of the neat ESO-CA polymer matrix, the ESO-CA-Au@PVP nanocomposites, and the aqueous dispersion of Au@PVP NPs are depicted in figure 4(a). Both the neat polymer and the nanocomposites showed an increase of the absorbance at short wavelengths ($\lambda < 450$ nm) due to the yellow-brownish coloration of the neat polymer matrix (figure 4(b)). For the ESO-CA-Au@PVP nanocomposites, an absorption band centered at 538–545 nm can be clearly distinguished, which correspond to the surface plasmon resonance of the NPs embedded in the polymeric matrix. The observed peak was slightly wider and red-shifted respect to that obtained for the aqueous dispersion of Au@PVP NPs. As reported by Liao *et al* for gold NPs of similar size [35], and as expected from the Mie theory [41], the presence of linear aggregates of gold NPs should produce the appearance of a second, red-shifted absorption band, associated to the longitudinal mode of the electronic plasma oscillation along the long axis of the gold NPs chains. This second mode could be responsible for the widening and red shift of the absorption band observed in the case of gold nanocomposites (figure 4(a)).

Zhang *et al* demonstrated that when photothermal heating is performed on a polymeric matrix containing gold NPs, it produces a temperature gradient [42]. The irradiated surface reaches the highest temperature and within a shorter timeframe than the inner layers, due to the high extinction coefficient and high heating rate of the gold NPs combined with the low thermal conductivity of the polymer. Figure 5 shows the variation of the temperature with time when ESO-CA-Au@PVP samples with high (5a) and low (5b) concentration of Au@PVP NPs were irradiated by a green laser with different values of the output power. A very quick response was observed in all cases, reaching the steady temperature in about 2 min after irradiation started. After irradiation ceased, a similar time range was needed for the sample to decrease back to room temperature. As expected,

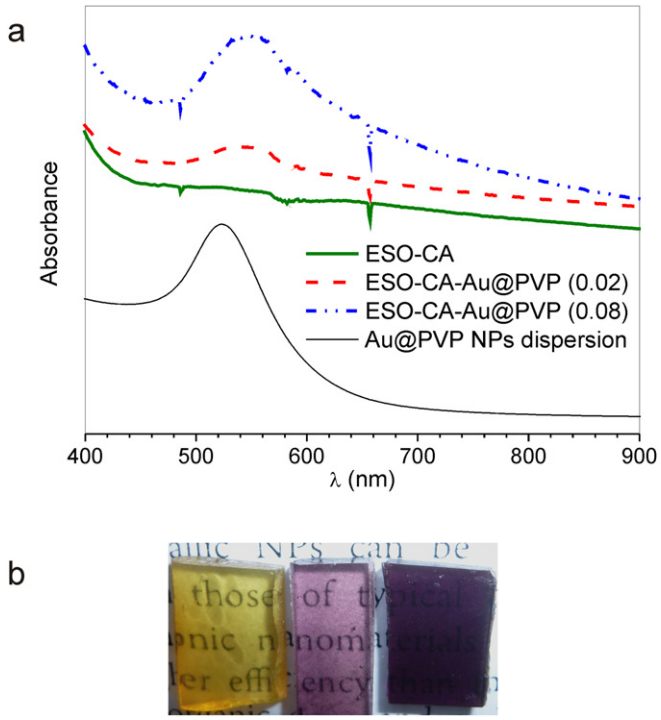

Figure 4. (a) UV–vis spectra of Au@PVP NPs aqueous dispersion, neat ESO-CA network and ESO-CA-Au@PVP nanocomposites. Curves are shifted vertically for the sake of clarity. (b) Picture of samples of ESO-CA neat polymer, ESO-CA-Au@PVP (0.02) and ESO-CA-Au@PVP (0.08), from left to right.

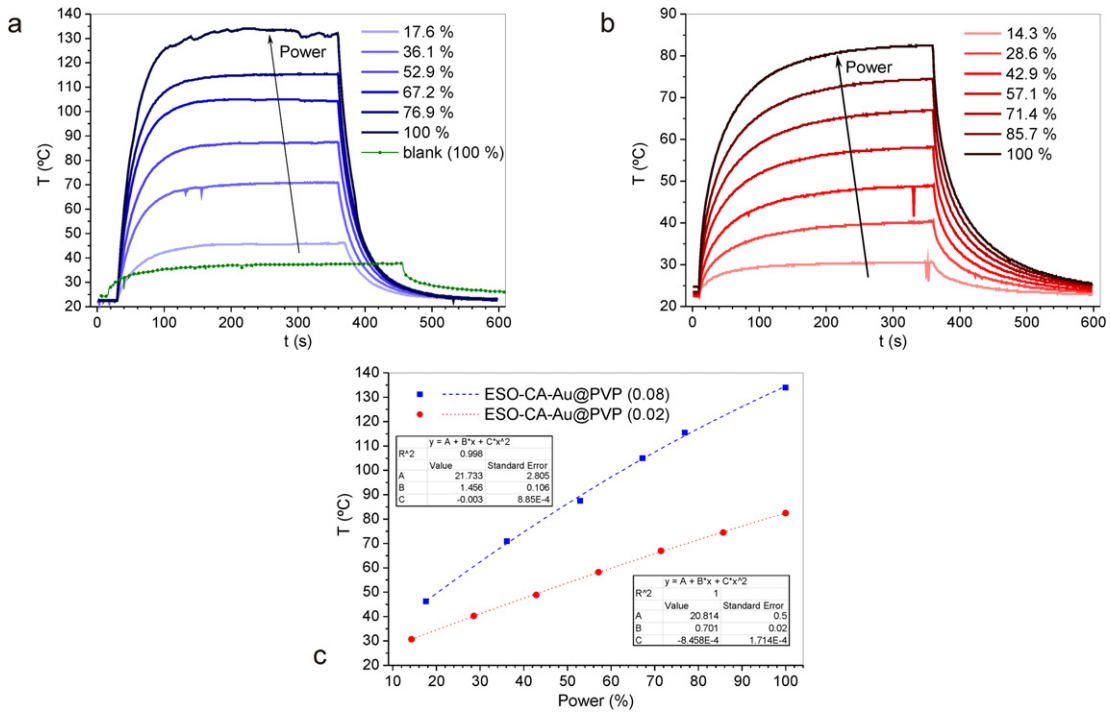

Figure 5. (a) Temperature versus time curves for different laser power values for the ESO-CA-Au@PVP (0.08), and for the ESO-CA neat polymer with the maximum power. (b) Temperature versus time curves for different laser power values for the ESO-CA-Au@PVP (0.02). (c) Steady temperature measured as a function of laser power for the composites with high and low NPs content. Laser power is expressed as percentage of the maximum power (700 mW).

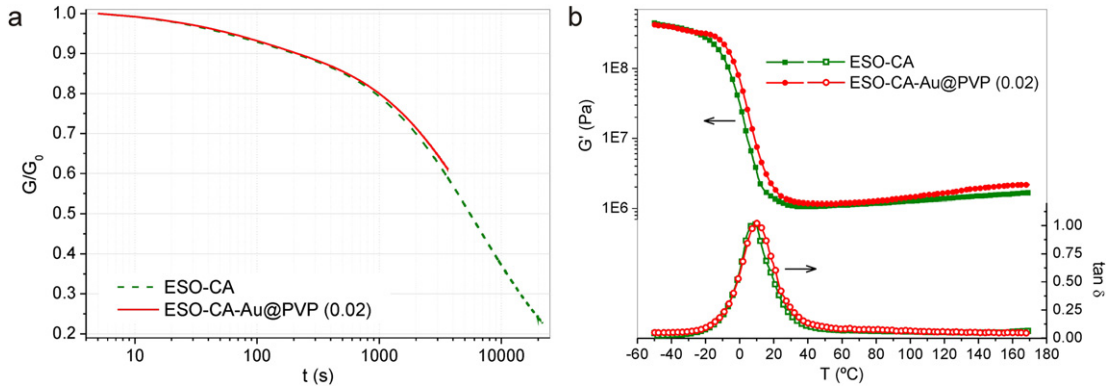

Figure 6. (a) Relaxation modulus (shown as G/G_0) as a function of time, and (b) storage modulus (G') and damping factor (tanδ) as a function of temperature for ESO-CA and ESO-CA-Au@PVP (0.02) nancocomposite.

higher temperatures were reached with higher laser outputs for the same sample, and for higher Au@PVP NPs concentration using similar irradiation intensity. A maximum steady temperature close to 132 °C was observed for the full power (700 mW) in the ESO-CA-Au@PVP (0.08) nanocomposite. However, it should be remarked that this temperature is the one measured by the thermocouple placed in the center of the specimen, but as it was explained before, the irradiated surface attains a higher temperature. Preliminary experiments carried out by an estimative measurement of the temperature at the surface of the plaque seem to confirm this fact. Indeed, under this condition a superficial degradation appeared in the area under direct irradiation, indicating that the temperature on the surface was above 200 °C (see supplementary data file). A similar measurement was performed in the neat ESO-CA network to use it as blank (figure 5(a)). Only a small temperature increase was detected even at maximum power, what was attributed to the yellow-brownish coloration of the sample.

The values of maximum temperature for each laser power for both systems are depicted in figure 5(c). The relation between temperature and laser power slightly deviates from a linear behavior for high laser power levels, which is similar to the correlation found by Zhang *et al* for the case of shape-memory hard hydrogels modified with gold NPs (2.5–10 nm of diameter) [31]. This nonlinearity could be ascribed either to a higher heat dissipation for higher temperatures, or to a nonlinear variation of the heat generation with the laser power.

The evaluation of photothermal triggered self-healing ability was performed on the ESO-CA-Au@PVP (0.02) system (instead of the nanocomposite with 0.08 wt% Au) in order to prevent the sample degradation due to the high temperatures achieved.

Stress relaxation and self-healing of ESO-CA networks when exposed to external heating in absence of any extrinsic catalyst was demonstrated in a previous work, as well as the possibility of reaching reasonable relaxation times in absence of degradation, for a temperature range comprised between 120 °C and 160 °C [13]. Stress relaxation experiments were performed on the ESO-CA-Au@PVP nanocomposites and compared with the ESO-CA systems, to evaluate any possible effect of the presence of gold NPs on the transesterification reaction rate. Figure 6(a) shows the stress relaxation behavior at 160 °C for both systems. A good overlapping of the curves can be observed, which would indicate the lack of significant effects of Au@PVP NPs on the kinetics of transesterification reactions (at least at the concentrations used in this work). Alpha-relaxation temperature (T_α) of the neat sample, obtained at the peak of the damping factor (tan δ) versus temperature curve, was 8 °C. As shown in figure 6(b), this value changed just slightly with the addition of Au@PVP NPs (tan δ peak was found at 10 °C). This low effect of the presence of NPs on T_α could be probably due to the moderately attractive interaction between PVP and the epoxy-acid network, the use of low metal concentrations and the morphology and big size of the elongated aggregates that eliminate the influence of confinement effects on T_α [43].

Figure 7 shows the first attempt to evaluate the healing capacity of a fractured sample of this material (picture (a)). The experimental set-up used to repair the sample is depicted in pictures (b) and (c). The sample was placed between a glass and a steel ring while two clamps were employed to assure a good contact between the healing surfaces (picture (b)), previous to the irradiation process with a green laser (picture (c)). The final healed sample after 1 h of irradiation is seen in (d). Figures 8(a) and (b)) shows pictures of a different sample healed by laser irradiation. The two pieces were held in contact with each other while irradiation was applied along the junction line on both sides (700 mW, 4 h on each side to irradiate the entire interface). The specimen could withstand a load of 100 g (0.98 N), corresponding to a tensile stress of 98 kPa considering the sample cross-section, which is a very promising result.

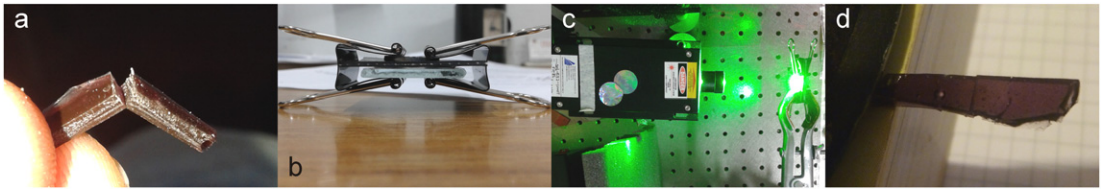

Figure 7. Series of pictures showing schematically the healing sequence of the ESO-CA-Au@PVP nanocomposites; (a) fractured sample; (b) sample held between a glass and a steel ring with two metallic clamps; (c) experimental set-up for the irradiation process; (d) repaired sample.

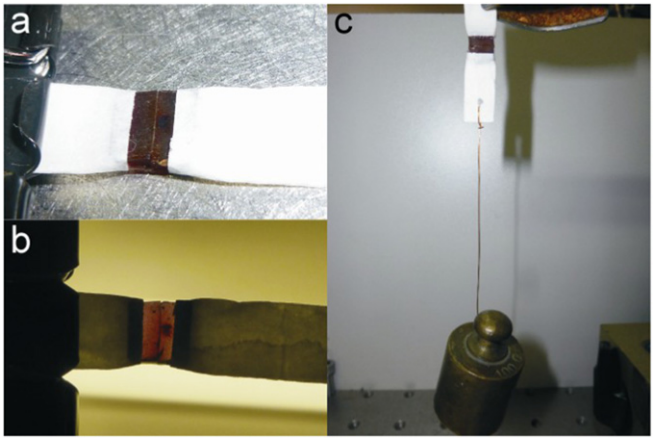

Figure 8. A repaired sample, with a cross-section of 7.2 × 1.4 mm^2, after complete break, obtained by irradiating for 4 h with a laser power of 700 mW. Pictures (a) and (b) show the sample, held with white adhesive tape. A visible scar is formed in the interface of the broken pieces. Picture (c) shows the repaired sample holding a weight of 100 g.

A different experiment was carried out with the aim of more realistically reproducing both the crack formation and propagation throughout the material in service as well as the healing procedure. A crack was initiated by bending a 2 mm thick sheet of ESO-CA-Au@PVP (0.02), and laser triggered reparation was performed by placing the cracked sample horizontally and without the aid of any external pressure. Here, it was assumed that crack faces became in close contact as a consequence of the difference in thermal expansion of the heated area respect to the non-irradiated one [29]. Figure 9 shows the TOM images of the crack before and after 2 h of irradiation with the maximum laser power (700 mW). The crack appears to be closed, and almost no visible marks are left in the area, indicating a good degree of healing even after a short irradiation time.

The mending efficiency was evaluated by tensile mechanical tests carried out on the samples healed without external pressure. Virgin specimens of the same material were used as control samples, and neat ESO-CA specimens were also tested for comparison purposes. It is worth to mention that according to the results shown in figure 10, the addition of Au NPs leads to an increase in the elastic modulus and to an improvement of the ultimate properties, such as the stress at rupture and the maximum extensibility. The increase in stiffness imparted by active fillers is reasonably well understood, and involves a hydrodynamic effect arising from the inclusion of rigid particles. However, as the particle concentration is very low, another effect must be evidently acting here. DMA tests (figure 6(b)), showed that the rubbery modulus does not change significantly with the addition of gold NPs for a given temperature. Therefore, according to the rubber elasticity theory, no significant change in the effective cross-linking density can be expected to explain the higher modulus and deformation at break observed in the tensile tests. Nevertheless, it should be noted that mechanical tests were performed at 18 °C, a temperature amidst the glass transition region for both the neat polymer and the nanocomposite, and also, as mentioned before, that the addition of Au NPs led to a slight increase in T_α. Hence, the apparent improvement in the mechanical performance can be ascribed to the mentioned change in T_α. Indeed, a difference of about 55% in the G' value was observed by DMA at 18 °C.

Remarkably, tensile tests also demonstrated that an excellent self-healing degree was attained. Figure 10 shows that the experimental curves obtained for the healed samples lie between two of the curves corresponding to the control specimens. The measured strength can be considered a quantitative assessment of the crack healing, and it also demonstrates its high efficiency. From these results it can be stated that, under this

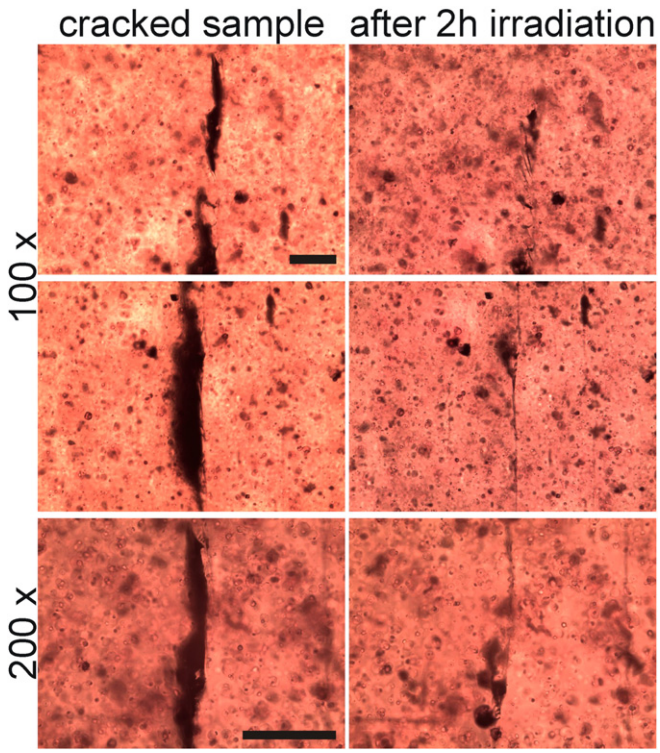

Figure 9. TOM images of a crack present in an ESO-CA-Au@PVP (0.02) sample, before and after being repaired by laser irradiation for 2 h. Scale bars lengths represent 0.2 mm.

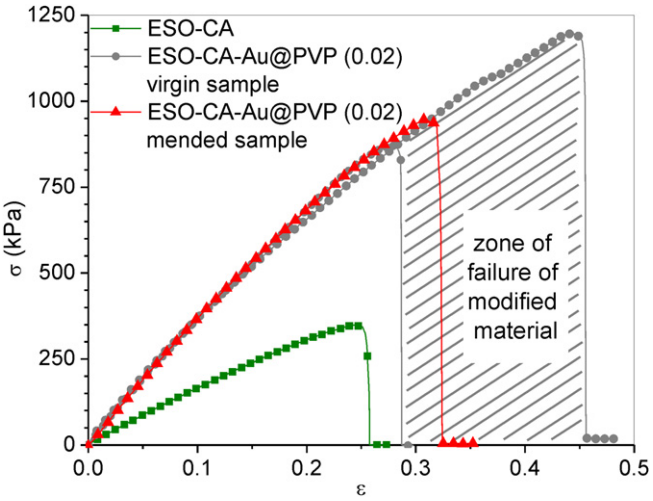

Figure 10. Representative stress–strain ($\sigma - \varepsilon$) curves for the ESO-CA network, ESO-CA-Au@PVP (0.02) virgin samples and ESO-CA-Au@PVP (0.02) mended samples.

conditions, the healing efficiency is in the order of 100%, being a proof of the effectiveness of the method presented herein.

Conclusion

Water soluble gold NPs were successfully incorporated in bio-based ESO-CA networks, by a simple procedure. Some linear aggregates are formed in the nanocomposites, probably due to electrostatic interactions that arise when the initial water is eliminated by evaporation and replaced by the much less polar ESO-CA pre-reacted system. These NPs aggregates allow the localized heating of the material by irradiation with a green laser, reaching temperatures well above 100 °C. This localized heating was harnessed to activate an efficient self-

healing of the material, with the great advantages of making possible remotely controlled reparation, without disassembling the damaged material, and with a much more efficient energy usage.

Acknowledgments

Authors would like to thank the National Research Council (CONICET), the National Agency of Scientific and Technological Promotion (ANPCyT) and the National University of Mar del Plata (UNMdP) for the funding. FIA also gratefully acknowledges the financial support from the Fundación Bunge y Born.

References

[1] Wu D Y, Meure S and Solomon D 2008 Self-healing polymeric materials: a review of recent developments *Prog. Polym. Sci.* **33** 479–522
[2] Yang Y and Urban M W 2013 Self-healing polymeric materials *Chem. Soc. Rev.* **42** 7446
[3] Billiet S, Hillewaere X K D, Teixeira R F A and Du Prez F E 2013 Chemistry of crosslinking processes for self-healing polymers *Macromol. Rapid Commun.* **34** 290–309
[4] Hayes S A, Jones F R, Marshiya K and Zhang W 2007 A self-healing thermosetting composite material *Composites* A **38** 1116–20
[5] Luo X, Ou R, Eberly D E, Singhal A, Viratyaporn W and Mather P T 2009 A thermoplastic/thermoset blend exhibiting thermal mending and reversible adhesion *ACS Appl. Mater. Interfaces* **1** 612–20
[6] Zhang J, Lin T, Cheung S C P and Wang C H 2012 The effect of carbon nanofibres on self-healing epoxy/poly(ε-caprolactone) blends *Compos. Sci. Technol.* **72** 1952–9
[7] Kessler M R and White S R 2001 Self-activated healing of delamination damage in woven composites *Composites* A **32** 683–99
[8] Hansen C J, Wu W, Toohey K S, Sottos N R, White S R and Lewis J A 2009 Self-healing materials with interpenetrating microvascular networks *Adv. Mater.* **21** 4143–7
[9] White S R, Moore J S, Sottos N R, Krull B P, Santa Cruz W A and Gergely R C R 2014 Restoration of large damage volumes in polymers *Science* **344** 620–3
[10] Zhang Y, Broekhuis A A and Picchioni F 2009 Thermally self-healing polymeric materials: the next step to recycling thermoset polymers? *Macromolecules* **42** 1906–12
[11] Zeng C, Seino H, Ren J, Hatanaka K and Yoshie N 2013 Bio-based furan polymers with self-healing ability *Macromolecules* **46** 1794–802
[12] Montarnal D, Capelot M, Tournilhac F and Leibler L 2011 Silica-like malleable materials from permanent organic networks *Science* **334** 965–8
[13] Altuna F I, Pettarin V and Williams R J J 2013 Self-healable polymer networks based on the cross-linking of epoxidised soybean oil by an aqueous citric acid solution *Green Chem.* **15** 3360–6
[14] Brutman J P, Delgado P A and Hillmyer M A 2014 Polylactide vitrimers *ACS Macro Lett.* **3** 607–10
[15] Lafont U, van Zeijl H and van der Zwaag S 2012 Influence of cross-linkers on the cohesive and adhesive self-healing ability of polysulfide-based thermosets *ACS Appl. Mater. Interfaces* **4** 6280–8
[16] Rekondo A, Martin R, Ruiz de Luzuriaga A, Cabañero G, Grande H J and Odriozola I 2014 Catalyst-free room-temperature self-healing elastomers based on aromatic disulfide metathesis *Mater. Horiz.* **1** 237
[17] Kuhl N *et al* 2015 Acylhydrazones as reversible covalent crosslinkers for self-healing polymers *Adv. Funct. Mater.* **25** 3295–301
[18] Ying H, Zhang Y and Cheng J 2014 Dynamic urea bond for the design of reversible and self-healing polymers *Nat. Commun.* **5** 3218
[19] Denissen W, Rivero G, Nicolaÿ R, Leibler L, Winne J M and Du Prez F E 2015 Vinylogous urethane vitrimers *Adv. Funct. Mater.* **25** 2451–7
[20] Habault D, Zhang H and Zhao Y 2013 Light-triggered self-healing and shape-memory polymers *Chem. Soc. Rev.* **42** 7244
[21] Govorov A O and Richardson H H 2007 Generating heat with metal nanoparticles *Nano Today* **2** 30–8
[22] Hühn D, Govorov A, Gil P R and Parak W J 2012 Photostimulated Au nanoheaters in polymer and biological media: characterization of mechanical destruction and boiling *Adv. Funct. Mater.* **22** 294–303
[23] Link S and El-Sayed M A 2000 Shape and size dependence of radiative, non-radiative and photothermal properties of gold nanocrystals *Int. Rev. Phys. Chem.* **19** 409–53
[24] Baffou G, Quidant R and Girard C 2009 Heat generation in plasmonic nanostructures: influence of morphology *Appl. Phys. Lett.* **94** 153109
[25] Gonçalves M R 2014 Plasmonic nanoparticles: fabrication, simulation and experiments *J. Phys. D: Appl. Phys.* **47** 213001
[26] Maity S, Downen L N, Bochinski J R and Clarke L I 2011 Embedded metal nanoparticles as localized heat sources: an alternative processing approach for complex polymeric materials *Polymer* **52** 1674–85
[27] Zhang H, Xia H and Zhao Y 2012 Optically triggered and spatially controllable shape-memory polymer–gold nanoparticle composite materials *J. Mater. Chem.* **22** 845–9
[28] Leonardi A B, Puig J, Antonacci J, Arenas G F, Zucchi I A, Hoppe C E, Reven L, Zhu L, Toader V and Williams R J J 2015 Remote activation by green-light irradiation of shape memory epoxies containing gold nanoparticles *Eur. Polym. J.* **71** 451–60
[29] Zhang H and Zhao Y 2013 Polymers with dual light-triggered functions of shape memory and healing using gold nanoparticles *ACS Appl. Mater. Interfaces* **5** 13069–75
[30] Zhang H, Fortin D, Xia H and Zhao Y 2013 Fast optical healing of crystalline polymers enabled by gold nanoparticles *Macromol. Rapid Commun.* **34** 1742–6
[31] Zhang H, Han D, Yan Q, Fortin D, Xia H and Zhao Y 2014 Light-healable hard hydrogels through photothermally induced melting–crystallization phase transition *J. Mater. Chem.* A **2** 13373
[32] Zillohu A U, Abdelaziz R, Hedayati M K, Emmler T, Homaeigohar S and Elbahri M 2012 Plasmon-mediated embedding of nanoparticles in a polymer matrix: nanocomposites patterning, writing, and defect healing *J. Phys. Chem.* C **116** 17204–9
[33] Kimling J, Maier M, Okenve B, Kotaidis V, Ballot H and Plech A 2006 Turkevich method for gold nanoparticle synthesis revisited *J. Phys. Chem.* B **110** 15700–7
[34] Kinge S, Crego-Calama M and Reinhoudt D N 2008 Self-assembling nanoparticles at surfaces and interfaces *ChemPhysChem* **9** 20–42
[35] Liao J, Zhang Y, Yu W, Xu L, Ge C, Liu J and Gu N 2003 Linear aggregation of gold nanoparticles in ethanol *Colloids Surf.* A **223** 177–83
[36] Kotov N A 2006 *Nanoparticle Assemblies and Superstructures* (Boca Raton, FL: Taylor & Francis/CRC Press)

[37] Reuter T, Vidoni O, Torma V, Schmid G, Nan L, Gleiche M, Chi L and Fuchs H 2002 Two-dimensional networks via quasi one-dimensional arrangements of gold clusters *Nano Lett.* **2** 709–11
[38] Pascault J-P and Williams R J J 2010 *Epoxy Polymers: New Materials and Innovations* (Weinheim: Wiley-VCH)
[39] Zucchi I A, Hoppe C E, Galante M J, Williams R J J, López-Quintela M A, Matějka L, Slouf M and Pleštil J 2008 Self-assembly of gold nanoparticles as colloidal crystals induced by polymerization of amphiphilic monomers *Macromolecules* **41** 4895–903
[40] Williams R J J, Hoppe C E, Zucchi I A, Romeo H E, dell'Erba I E, Gómez M L, Puig J and Leonardi A B 2014 Self-assembly of nanoparticles employing polymerization-induced phase separation *J. Colloid Interface Sci.* **431** 223–32
[41] Galletto P, Brevet P F, Girault H H, Antoine R and Broyer M 1999 Enhancement of the second harmonic response by adsorbates on gold colloids: the effect of aggregation *J. Phys. Chem.* B **103** 8706–10
[42] Zhang H, Xia H and Zhao Y 2014 Light-controlled complex deformation and motion of shape-memory polymers using a temperature gradient *ACS Macro Lett.* **3** 940–3
[43] Srivastava S and Basu J K 2007 Experimental evidence for a new parameter to control the glass transition of confined polymers *Phys. Rev. Lett.* **98** 165701